Numerical Analysis and Simulation Analysis for Space-Time Data

M. A. Hassouba[*1]**, H. I. Al-Naggar**[1]**, N. M. Al-Naggar**[1]**,** and **C. Wilke**[2]

[1] Department of Physics, Faculty of Science, Benha University, Egypt.
[2] Institute of Physics, E. M. A. University, Domstr. 10a, 17489 Greifswald, Germany

Spatio temporal dynamics of the positive column of a dc neon glow discharge is studied and investigated experimentally and theoretically. Spatio temporal analysis by means of biorthogonal decomposition method (BOD) gives insights into the mechanism of irregularity and can be employed for characterization of spatio- temporal complexity. In the weak nonlinear region, the wave dynamics is approximated by an amplitude equation of the Ginzburg-Landau equation (CGLE) with complex coefficients and an additional integral term based on a fluid model. In the present work we deal with irregular spatio-temporal data. A comparison between the numerical analysis of the experimental data and simulation results are studied. A good agreement between the dynamical behaviour for experimental space-time data and theoretical simulation space-time results was obtained.

1 Introduction

Extended dissipative systems far from equilibrium may exhibit complex spatio-temporal dynamics (STD) leading to the formation of regular patterns and/or turbulence, respectively [1]. In discharges, which may be considered as field affected reaction-diffusion systems, non-linear wave states may occur in the positive column if a control parameter, e.g. the discharge current I is increased above a threshold value leading to a Hopf bifurcation [2]. Here, the Hopf patterns represent ionization waves yielding a modulation of the light emerging from the discharge [3]. The aim of the present work is to investigate the irregular patterns of space-time data of ionization waves in the dc neon glow plasma. The patterns would be characterized both experimentally and theoretically. The analysis of the dynamics is performed by means of two methods numerical method and simulation method.

The experimental work [4] is performed in a cylindrical dc glow discharge tube with r =1 cm, discharge length $L = 60$ cm, and $I < 60$ A. The striations can be observed by the light emission of excited atoms in the positive column by means of a charge-coupled device (CCD), see Fig. 1.
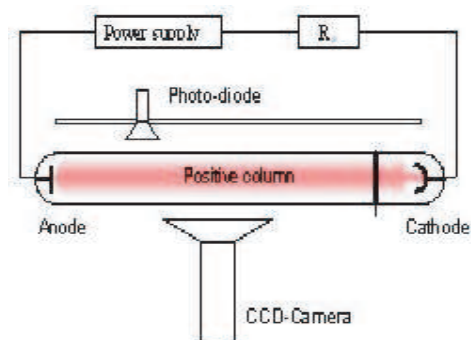

Fig. 1 Experimental set-up. The light fluctuations are recordet with CCD-Camera.

[*]Corresponding author: e-mail: hassouba@yahoo.com

2   Theoretical background

2.1   A numerical model

Let $u(x,t)$ be a physical quantity measured simultaneously in M space positions x_j, and the signal is sampled at n times t_i, where x and t denote space and time variables [5]. This physical quantity is decomposed by the biorthogonal decomposition (BOD) method. The BOD is mathematically equivalent to Singular Value Decomposition (SVD) method, which is known as Karhunen-Loeve or proper orthogonal decomposition. The BOD is employed to characterize the spatio-temporal data and to analyze the wave dynamics.

The experimental spatio-temporal data can be written as a matrix [5]:
$$U_{ij} = u(x_j, t_i), \quad i = 1, \ldots, N, j = 1, \ldots \ldots, M(N > M).$$
Also the above equation can be expanded into orthogonal modes as [5]:

$$U_{ij} = \sum_{k=1}^{K} A_k \psi_k(t_i) \varphi_k(x_j), \quad \text{with} \quad k = min(N, M). \tag{1}$$

where, $A_1 \geqslant A_2 \geqslant \ldots \geqslant A_k > 0$, and A_k are called the weights. The spatial eigen modes φ_k are called *Topos*, and the temporal eigen modes ψ_k are called *Chronos*. The decomposition is unique and is always possible. The main purpose of this decomposition is to derive a weighted set (weights A_k) of eigen functions in space (*Topos* $\varphi_k(x)$) and time (*Chronos* $\psi_k(t)$) [5].

From the BOD method, it is noticed that [6], U is decomposed into a set of orthogonal sets of modes; each *Topo* always corresponds to a single *Chrono*. This makes the BOD a powerful tool for the detection of spatio-temporal coherences that are indicated by degenerated modes, i.e., modes $\varphi_\kappa A_\kappa \psi_\kappa$ with the same weight.

The energy of the kth mode can be defined as [6]:
$$E_k = \frac{A_k^2}{\sum\limits_{k=1}^{K} A_k^2} = p_k \quad 0 \leqslant p_k \leqslant 1 \text{ and } \sum_{k=1}^{K} p_k = 1.$$
The dimension $D_{BD}(L)$ can be defined as [6]:

$$D_{BD}(L) = \exp\left\{-\sum_{k=1}^{L} p_k \ln p_k\right\}.$$

where, L is the length of the positive column region, and D_{BD} is the dimension of the biorthogonal decomposition. The chronos and topos represent a least –square optimized real orthonormal basis of the N- and M- dimensional finite spaces of space (length L) and time (length T) observation, respectively. Also the chronos describe the temporal activity of the associated spatial eigen mode. Spatio-temporal analysis by means of BOD method gives insights into the mechanism of irregularity and can be employed for characterization of spatio-temporal complexity [7]. Here the BOD method is used to study the dominating degenerated spatial eigen modes, which indicate the positions of wave activity along the discharge length.

2.2   Comparison with an amplitude equation

The amplitude equation describes the slowly varying complex amplitude $A(z,t)$ of the ionization waves which is given as follows [8]:

$$\begin{aligned}
\frac{\delta A}{\delta t} = {}& \varepsilon^2 p_r A - v_g \frac{\delta A}{\delta z} + b \frac{\partial^2 A}{\partial z^2} + c A^* A^2 + d A^{*2} A^3 \\
& + \left(a - i\frac{\delta c}{\delta k}\bigg|_o\right) A \frac{\delta A^* A}{\delta z} - i\frac{\delta c}{\delta k}\bigg|_o A^* A \frac{\delta A}{\delta z}
\end{aligned} \tag{2}$$

This equation is the final form of the amplitude equation with the unfolding parameter [8]:

$$\mu = p_r \varepsilon^2 = p_r \frac{I_o - I_c}{I_c}, \quad v_g = \frac{\delta \omega_c}{\delta k_c}$$

$$b = b_r + ib_i, \ \ c = c_r + ic_i, \ \ a = a_r + ia_i, \ \ d = d_r + id_i. \tag{3}$$

The coefficients can be calculated at different plasma parameters [9]. In equation (3) the index r means a real part, and i stands for the imaginary part of the complex coefficients. We [10] can eliminate the term v_g by means of a Galilei transformation. Moreover, scaling transformations are possible such that $b_r \rightarrow 1$, $c_r \rightarrow -1$ and $\varepsilon^2 p_r \rightarrow 1$.

In order to solve equation (2), we take the observable quantities $\psi(z, t)$ in the discharge plasma which is given by:

$$\psi(z,t) = \psi_o[A(z,t) \exp i(kz - \omega t) + c.c] \tag{4}$$

where, ψ_o is a constant factor, k is the critical wave number and ω is the frequency at the bifurcation point. The complex amplitude $A(z, t)$ can be given as [10]:

$$A(z,t) = |A| \exp i[\varphi(z,t)]. \tag{5}$$

Our main objective here is to solve the amplitude equation (2) by inserting equation (4) with simulation C^{++} program. We can calculate $A(z, t)$ theoretically and save it as a matrix of two dimensions as experimental data.

3 Results and discussion

The first four BOD modes for the first 50 ms from irregular experimental space-time data are represented in Fig. 2. The original data image is shown in the left panel of the upper row of the figure. The first mode can be clearly identified as the ionization wave corresponding to the dominant mode of the positive column. This mode was found to decrease when spatio-temporal dislocations appear. For these times, the mode activity of the next three modes switches to different regimes indicating a side-band activity during these periods, as these side bands can be identified as spatial eigen modes, the occurrence of dislocations is due to a non-linear interaction of spatial wave modes. Figure 2 shows also the weights plotted versus number of modes. The doublets at small index numbers except $n = 1$ mode indicate spatio-temporal coherences. The results displayed in Fig. 2 show that the first eight weights represent four doublets except $n = 1$ mode. The first four modes govern the spatio-temporal dynamics, i.e., they are enough for reconstruction of the experimental image. For higher indices complexity can be derived from the scaling of the weights as displayed in the inset of Fig. 2, and the larger the highindex weights, the more complex is the spatio-temporal pattern. The time series of the time wave function (chronos analysis) for each mode from Fig. 2 are displayed in Fig. 3, which represent three different type waves for the ionization wave. The behaviour of the PSD for the four modes are represented in Fig. 4, which denotes irregularity behaviour for each mode where the PSD behaviour is smooth and continuously decaying with increasing frequency and maybe give a chaotic attractor. The spatial wave functions (Topos analysis) as a function of discharge length are represented in Fig. 5. The amplitude of oscillation increases towards the anode and vanishes at the column head (cathode region) at position $x \leqslant 5$ cm for modes 1, 2 and 3 but for mode 4 vanishes at $x \leqslant 1$ cm. Additionally, from this figure the interval region $20 \leqslant x \leqslant 50$ cm exhibits a larger oscillation amplitude. From BOD analysis, one can see that the instability state of space-time plasma comes from the non-linear behaviour of the spatial wave-wave interaction.

For the simulation image, the 50 ms were calculated and represented in Fig. 6. The original data image is shown in the left panel of the upper row of the figure. Mode 1 indicates a regular wave. BOD modes become active when the first BOD mode appears to be blurry. From the weights figure, it is clear that the first four modes are enough to reconstruct the original image. Figure 7 represents the time series for the time wave function for each mode. The Chronos analysis behaviour shows the amplitude turbulence, which may be a chaotic attractor near the anode region. The PSD's corresponding to each mode are represented in Fig. 8. The behaviour of PSD gives a more broad band and decreases with the increasing frequency. Figure 9 shows that, the amplitude of oscillation increases towards the anode for modes 2, 3 and vanishes at the column head (cathode region) at position $x \leqslant 1$ cm, while mode 1 has an approximate constant oscillation.

On the other hand, the time series analysis for both experimental space-time data and simulated space-time data are calculated. We extract the time series at distance 45 cm near the anode region of the positive column from the two images (experimental space-time image and simulated space-time image). After that, a comparison

between the correlation dimension and Lyapunov exponents for the two data is given. One can note that the time series analysis gives the temporal analysis for all modes (chronos analysis).
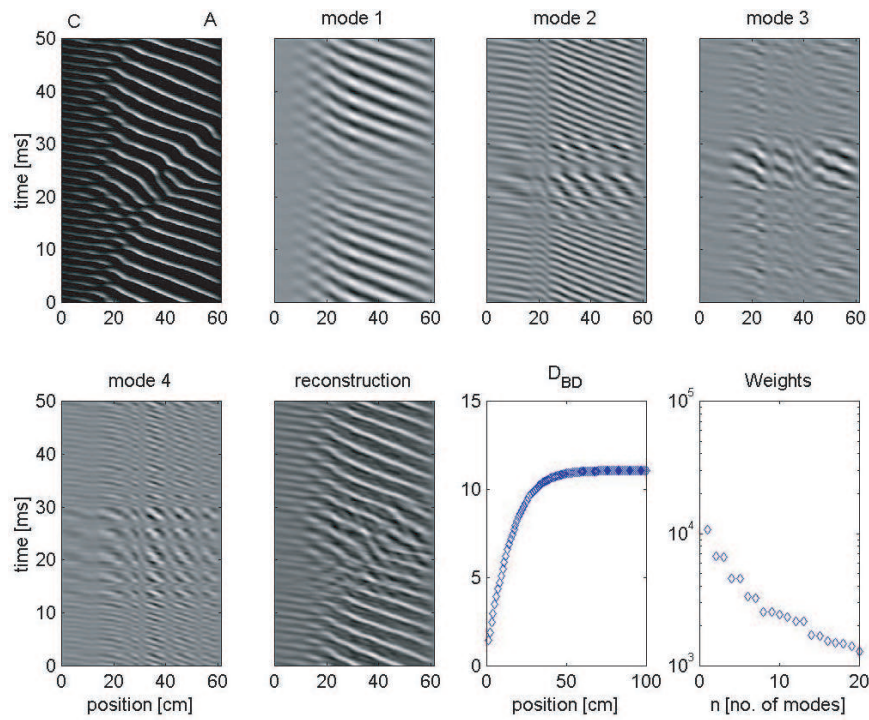

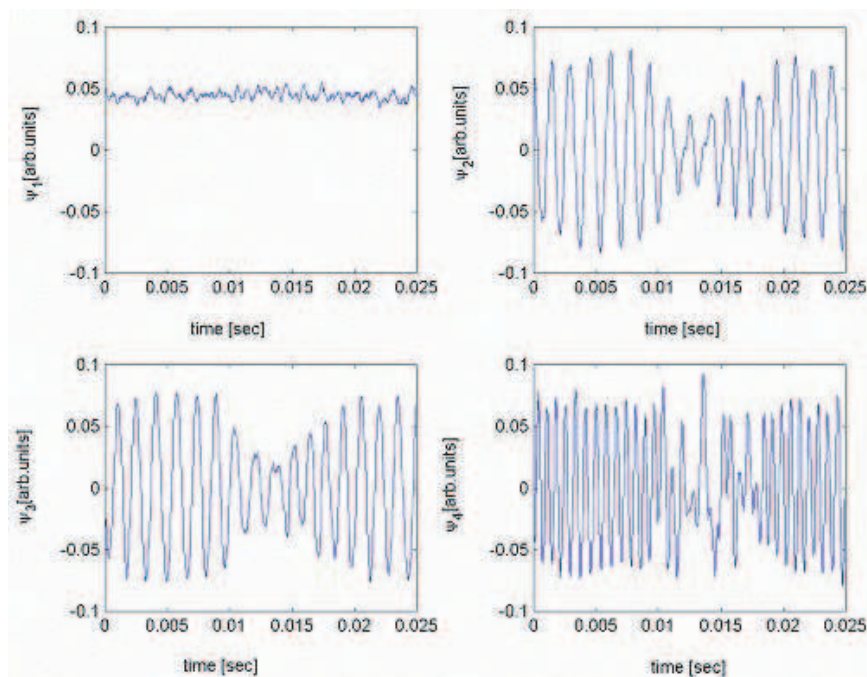**Fig. 2** The four first BOD modes for experimental space-time data.

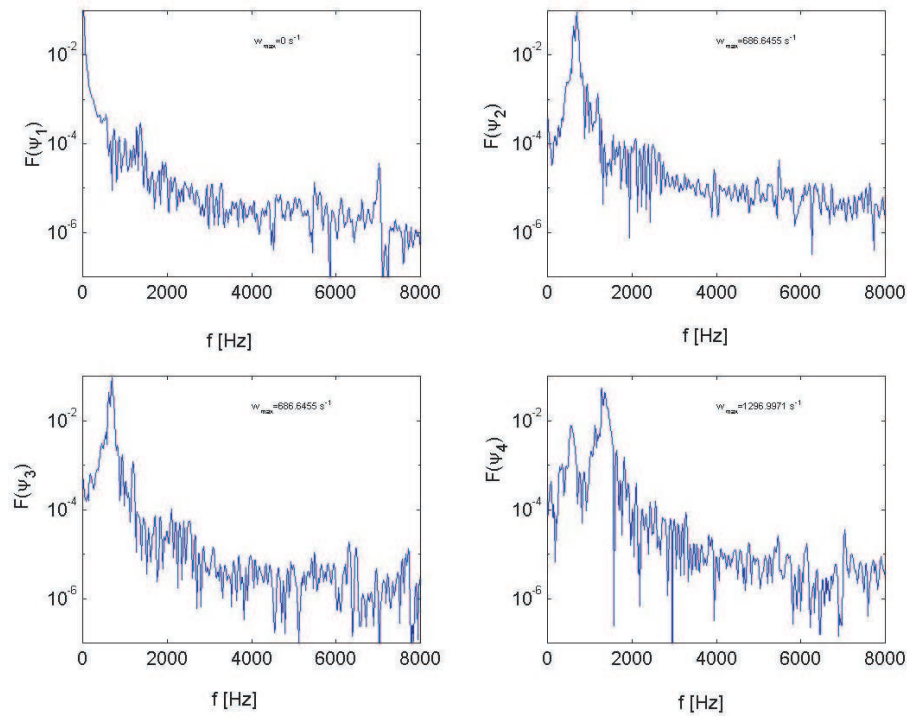**Fig. 3** CHRONOS analysis for the first four BOD modes for experimental data.
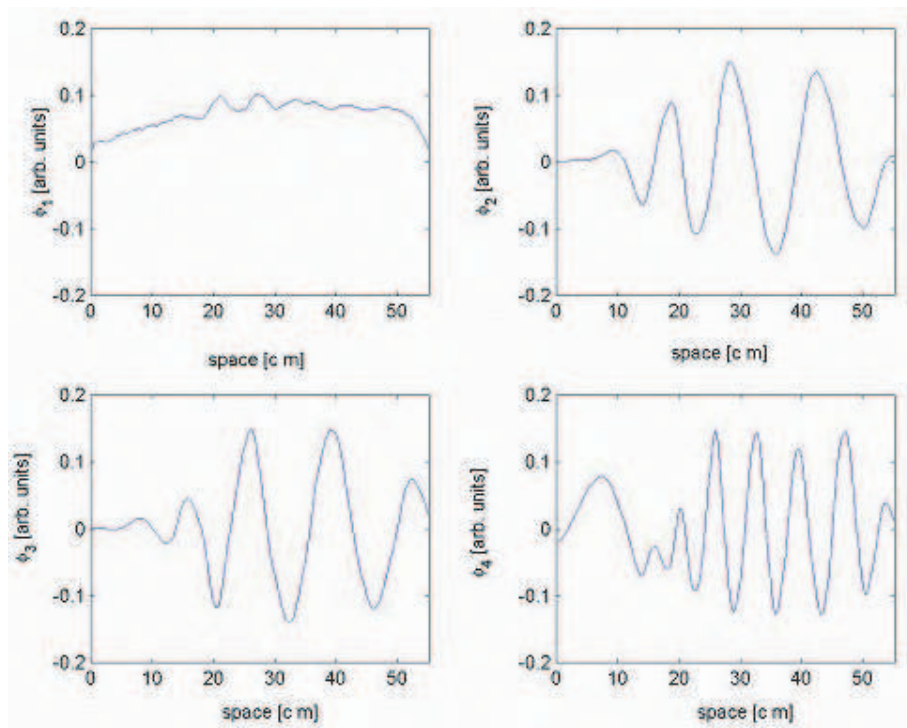
Fig. 4 PSD for each time series for each mode of Fig. 3.
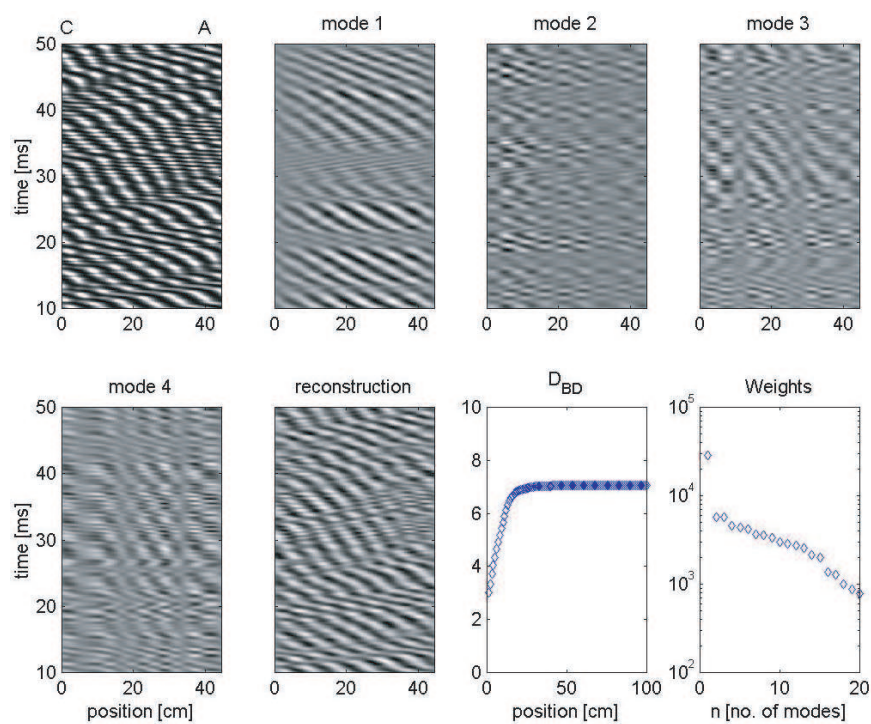

Fig. 5 Spatial analysis (TOPOS analysis) for experimental space-time data.

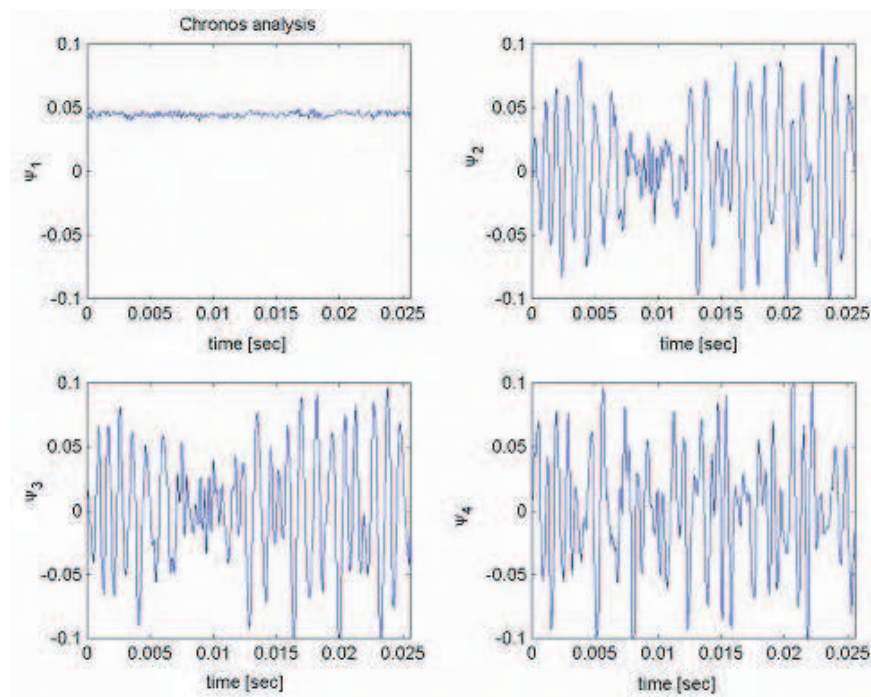**Fig. 6** Spatial analysis (four first BOD modes) for simulated space-time data.

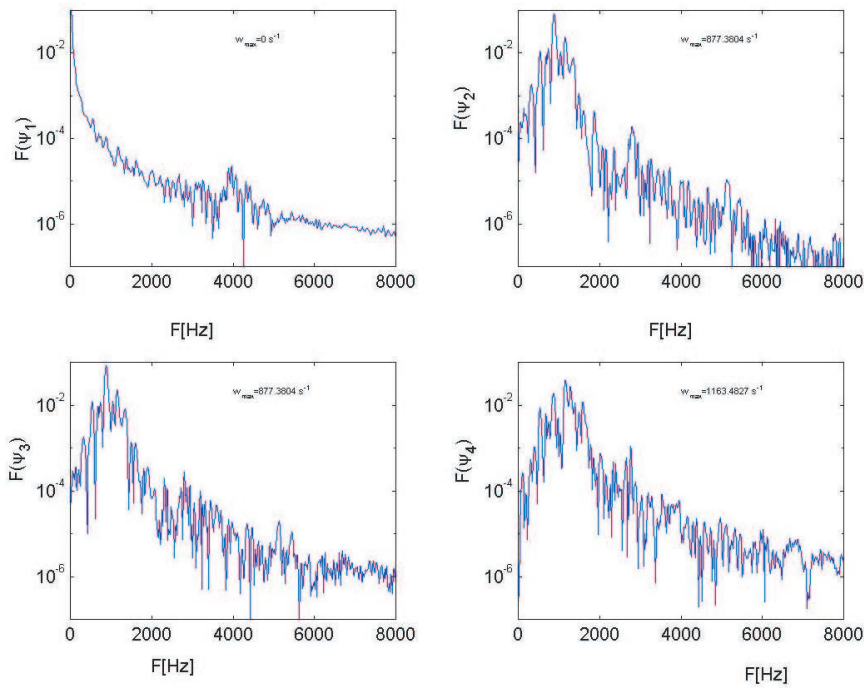**Fig. 7** Spatial analysis (CHRONOS analysis) for each mode in Fig. 6.

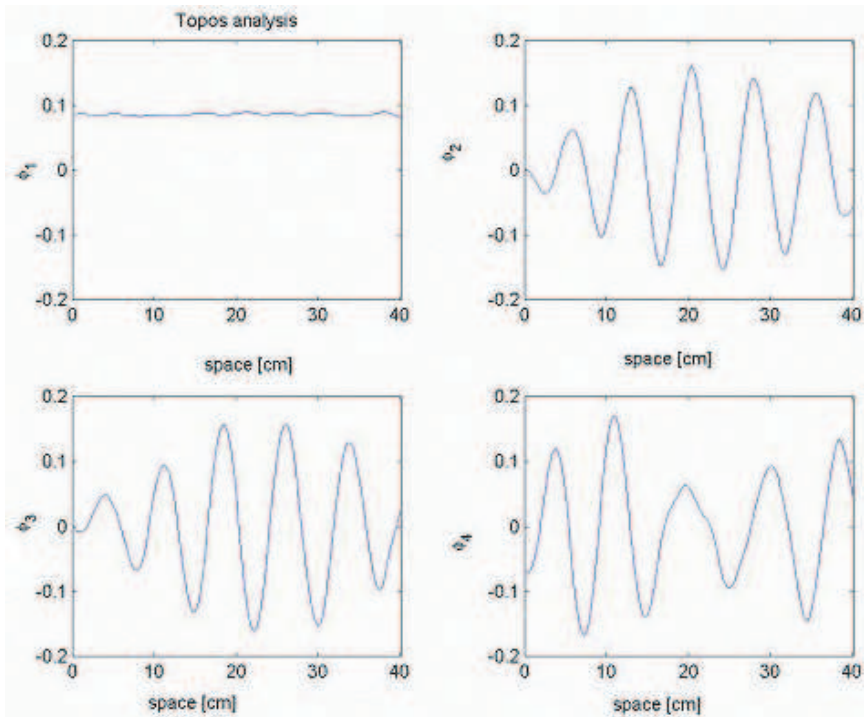**Fig. 8** Spatial analysis (the power spectrum density (PSD)) for time series in Fig. 7.

Fig. 9 Spatial analysis (spatial wave function for each BOD mode) for simulated space-time.

The autocorrelation function (ACF) calculations for experimental space-time data and theoretical space-time results are represented in Fig. 10. A good agreement between the experimental and theoretical data is obtained, and shows a chaotic attractor. This result is supported by LES and D_{corr} calculations. The LES for simulated results can be identified as $(+,0,-,-)$, which indicates a chaotic attractor, and is displayed in Fig. 10b, c, with the value of $D_{KY} = 2.8$. The LES for experimental data can be identified as $(+,0,-,-)$, which gives also a chaotic attractor and has the same value for D_{KY}. The D_{corr} calculation for experimental and theoretical space-time data are represented in Fig. 11. The values give fractal dimensions, i.e., give a chaotic attractor. This behaviour is clear in the PSD for four modes of all space-time data (the experimental and the theoretical space-time data).
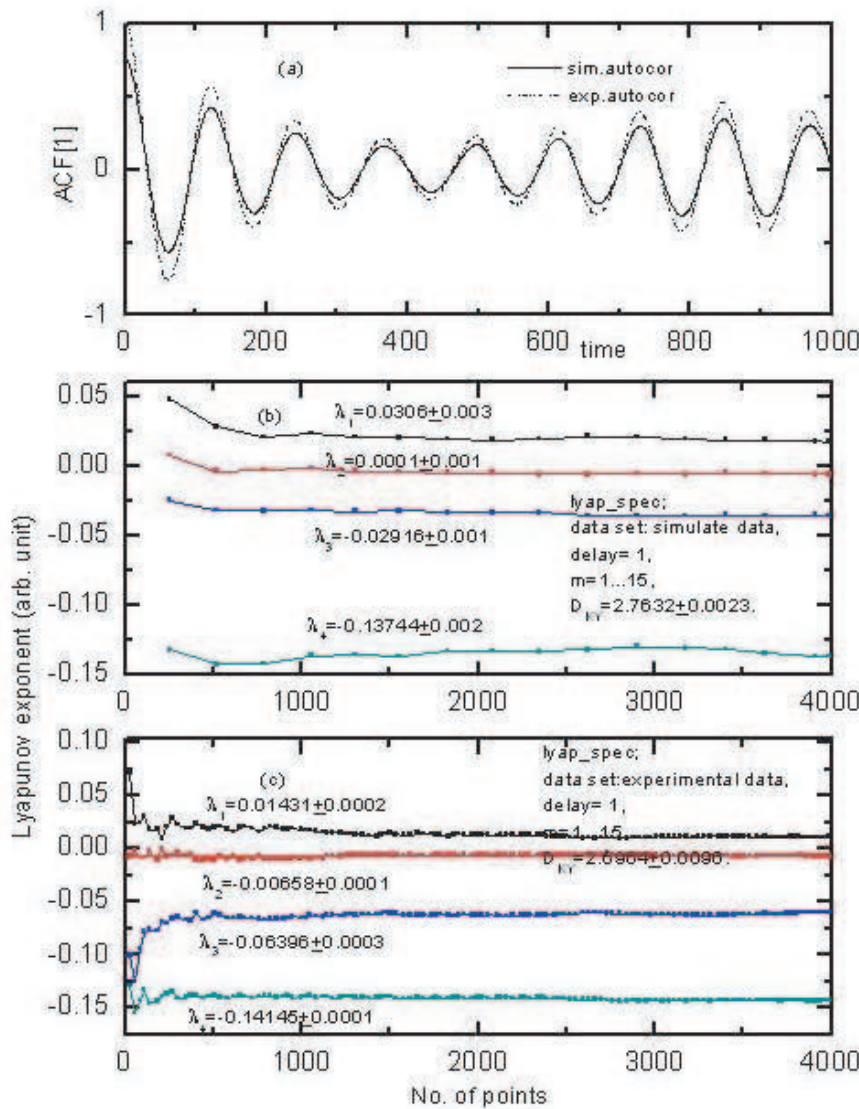

Fig. 10 Autocorrelation function and Lyapunov exponents for simulated space-time data and experimental space-time data.

Finally, the simulation results for the amplitude equation are in good agreement with the experimental space-time data. The amplitude equation is a good method for theoretical analysis of weak non-linear glow discharge systems that deal with the glow discharge as a fluid system and also as a wave-wave interaction.

From the time series analysis, a good agreement between the theoretical simulation space-time data and experimental space-time data is obtained as shown in Figs. 10 and 11.
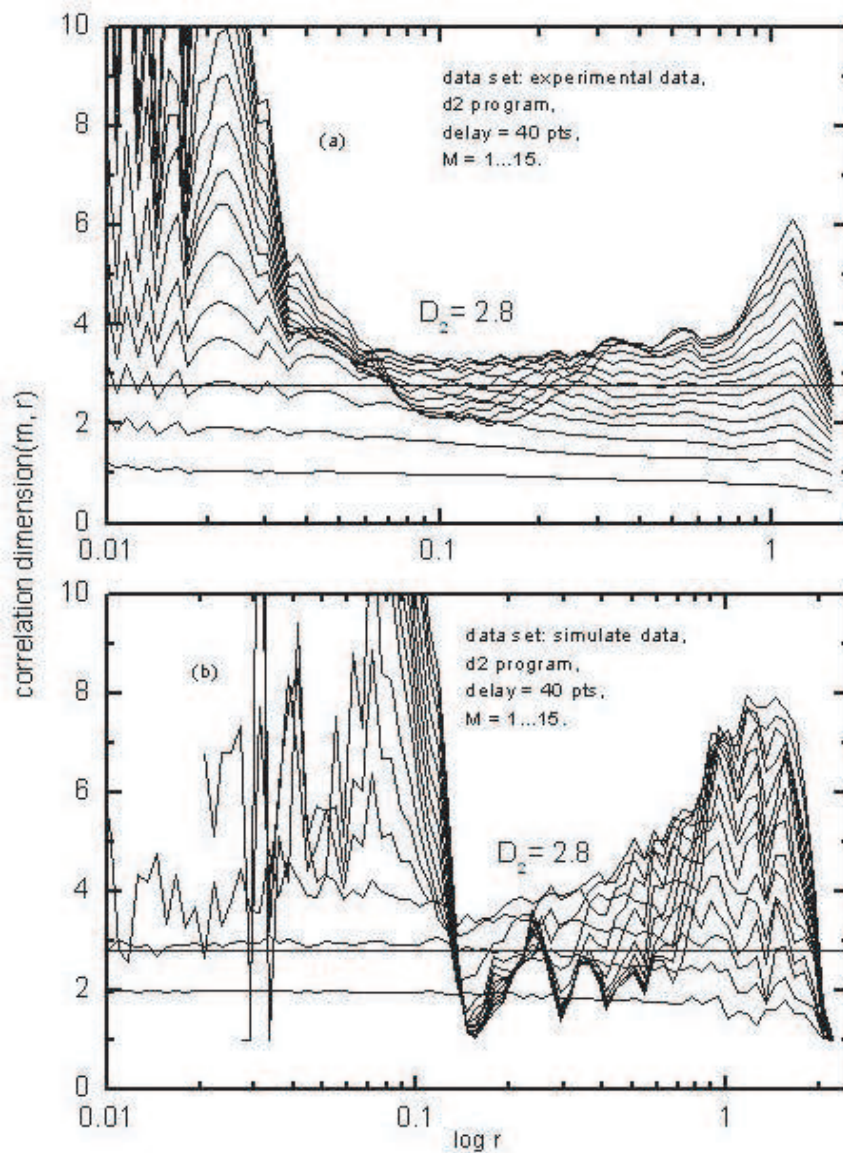
Fig. 11 Correlation dimensions for both experimental time series and theoretical time series.

References

 [1] M.C. Cross and P.C. Hohenberg, Rev. Mod. Phys. **65** , 851 (1993).
 [2] A. Dinklage, C. Wilke, G. Bonhomme and A. Atipo, Phys. Rev. E **62**, 7219 (2000).
 [3] N.L. Oleson, and A.W. Cooper, Adv. Electron. Phys. **24**, 155 (1968).
 [4] C. Letellier, A. Dinklage, H. Al-Nagger, C. Wilke and G. Bonhomme, Phys. Rev. E **63**, 1 (2001).
 [5] N. Aubry, F. Carbone, R. Lima and S. Slimani, J.Stat. Phys. **76**, 1005 (1994).
 [6] A. Dinklage, P. Jonas, C. Wilke, G. Bonhomme, and A. Atipo, ECA **22C**, 2338 (1998).
 [7] A. Dinklage, C. Wilke, G. Bonhomme and A. Atipo, Phys. Rev. E **62**, 7219 (2000).
 [8] B. Bruhn and B.P. Koch, Phys. Rev. E **61**, 3078 (2000).
 [9] P. Jonas, B. Bruhn, B.P. Koch and A. Dinklage, Physics of Plasmas **7**, 729 (2000).
[10] B. Bruhn, Physics of Plasmas **11**, 4446 (2004).